P3.1 ANALYSIS OF THE DOWNWARD TRANSPORT IN RICO OBSERVATIONS

Thijs Heus*, C. Freek J. Pols, Harm J. J. Jonker, and Harry E. A. van den Akker
Multi-Scale Physics, Delft University of Technology, The Netherlands
and Donald H. Lenschow,
National Center for Atmospheric Research, Boulder, Colorado

ABSTRACT

The existence of a subsiding shell around cumulus clouds has been observed before in several aircraft measurement campaigns. Recent results from large-eddy simulations (LES) pointed out that the downward mass flux through the shell compensates a significant fraction of the upward mass flux through the cloud. In this study, airplane measurements from the Rain In Cumulus over the Ocean (RICO) field campaign are used to verify this compensating mass flux. Just like in the LES results, the in-shell mass flux is found to be significant. However, a few differences were found in comparison with the LES results; most of them were explained by taking into account the difference between the 2-dimensional slabs in LES and the 1-dimensional lines from airplane observations.

1. INTRODUCTION

The interaction between a shallow cumulus cloud and its environment has been a popular research topic for more than half a century. A significant part of the discussion has dealt with the significance of either cloud-top mixing or lateral mixing. Evidence for each mechanism has been shown both in modeling (e.g., Stommel, 1947; Squires, 1958; Asai and Kashara, 1967) as well as in observational studies (e.g., Paluch, 1979; Blyth et al., 1988; Taylor and Baker, 1991). In the same vein, Jonas (1990) and Rodts et al. (2003) investigated the behavior of the subsiding shell of descending air around cumuli, which was also studied by Grabowski and Clark (1991, 1993a,b) in an analysis of the cloud-boundary instability in a stably stratified (but possibly sheared) environment.

More recent studies attributed a larger significance to the shell than was inferred from previous works: Observations by Siebert et al. (2006) showed that the shell is associated with increased turbulence around the cloud edge. Gerber et al. (2008) pointed out that the shell increases the humidity and lowers the temperature the air or, in other words, *pre-conditions* the air entrained into the cloud. Both the increased turbulence and the preconditioning may lead to more homogeneous mixing at the edge of the cloud and shift the droplet size distribution toward smaller sizes. Heus and Jonker (2008) found that the shell is able to compensate a significant portion of the in-cloud mass flux. This point was further elaborated by Jonker et al. (2008, hereafter JHS08) who stated that around 80% of the in-cloud mass flux was compensated within $200\,\mathrm{m}$ of the edge of the cloud. Thus, the importance of the shell in cloud dynamics was increased from a mere marker of mixing dynamics to a significant contributor to the droplet size distribution and to the balance of mass in a cloud field.

The large mass flux found by JHS08 in comparison with the previous studies was attributed to three factors. First, compositing data with respect to cloud edge instead of cloud center (which is more common) enabled JHS08 to better focus on the shell. Second, the determination of the nearest cloud was done in the 2-dimensional horizontal plane rather than along the airplane track only. This means that clouds alongside a flight track can also be accounted for; this significantly decreases the distance to the nearest cloud. Third, consideration of the mass flux rather than the vertical velocity better delineated the differences in area between cloud core, shell and far environment. This was a crucial point in the argument of JHS08, since the area of the shell is proportional to the perimeter of a cloud. This means that the area of the shell is significant compared with the area of the cloud. Since mass flux is equal to vertical velocity integrated over area, the mass flux in the shell is easily underestimated.

In this study, we pursue verification of the numerical results of JHS08 by means of observations. To this end, we apply the JHS08 methodology to the airplane observations from the Rain In Cumulus over the Ocean (RICO) field campaign (Rauber et al., 2007a).

Our comparison of simulations and observations is two-staged. As argued above, a 2-dimensional view of the horizontal plane is necessary to fully appreciate the downward mass flux in the shell. Ideally speaking, we would like to validate the 2D results from LES directly with 2D observational data. Since such 2D observations are not available, we analyse the LES data set twice: Once from a 2D point of view, strictly following JHS08's method, and a second time, from a 1D point of view. The latter method is prone to several biases, as JHS08 argued, but the 1D observations are prone to the same biases. This means that a reliable *validation* can be performed by comparing the 1D LES results with the observations. If this validation is successful, this gives credence to the 2D LES results.

The details of the methodology are described in section 2, along with a discussion of the observational data. The validation of JHS08 is discussed in section 3, the up- and downdrafts are more generally treated in section 4 and some implications are briefly addressed in section 5.

* *Corresponding author address:* Harm Jonker, Dept. of Multi-Scale Physics, Delft University of Technology, Delft, The Netherlands (h.j.j.jonker@tudelft.nl - www.msp.tudelft.nl)

Table 1: Some specifications of the analyzed flights.

Flight	Date	Cloud base (m)	Flight heights (m)		
RF01	Dec 7	650	830	1940	
RF03	Dec 9	450	830	1470	
RF04	Dec 10	570	650	980	1320
RF05	Dec 13	300	780	1090	1440
			1780	1880	
RF06	Dec 16	550	640	730	790
			900	980	
RF09	Dec 20	480	660	830	910
			1050	1150	1270
			1360	2000	
RF10	Jan 5	680	840	980	1160
			1320	1620	
RF12	Jan 11	600	800	850	1000
			1180	1480	1640
RF13	Jan 12	400	770	1950	

2. DATA DESCRIPTION AND METHODOLOGY

We use data collected by the NSF/NCAR C130 airplane in the RICO campaign. Details of the campaign in general and of the flight plan in particular have been described in Rauber et al. (2007a) and Rauber et al. (2007b); a short summary of the relevant information is given here.

The data was obtained between December 7, 2004 and January 12, 2005 (see Table 1 for some details). Each flight contains several semirandom trajectories at fixed altitudes with a duration of $30 - 60\,\mathrm{min}$. The term 'semirandom' implies that smaller clouds and the environment are fairly well represented in the ensemble, although the pilot attempted to transect active clouds, aiming at their center. Droplet number density was measured with the NCAR FSPP-100, a PMS Forward Scattering Spectrometer Probe with a sample rate of $10\,\mathrm{s}^{-1}$. Velocities were obtained at $25\,\mathrm{Hz}$ from navigation information and pressure differences measured with a five-hole system on the aircraft radome. Temperature was measured with a Rosemount thermometer at $25\,\mathrm{Hz}$.

A transect is defined as cloudy if the droplet number density continously exceeds $7\,\mathrm{cm}^{-3}$ (see Rodts et al., 2003). Velocity and temperature are downsampled and interpolated where necessary to $10\,\mathrm{Hz}$ to match the frequency of droplet number observations. Combined with the average cruise speed of the C130 of $106\,\mathrm{m\ s}^{-1}$ this results in a spatial resolution of $10.6\,\mathrm{m}$. Before further processing, the average vertical velocity of each observational leg is subtracted from the ensemble.

Since the main aim of this study is to validate the mass flux distribution as observed by JHS08, we follow their method of compositing with reference to the cloud edge as closely as possible. For all samples $i = 1...N(z)$ along a fixed-altitude track the distance r_i to the nearest cloud edge has been determined. For in-cloud samples, r_i is taken to be negative, and for environmental samples r_i is defined positive. This horizontal distance to the cloud edge is analogous to what Lenschow et al. (2000) used to study cloud-top entrainment in stratocumulus. Note that we deviate here from JHS08's method; they determined the distance r to the cloud edge in 2D, whereas the airplane data only allows for a 1D calculation of this distance.

The number density $n(r)$ of the entire cloud field is defined as:

$$n(r) = \frac{1}{N(z)\Delta r} \sum_{i=1}^{N(z)} \sqcap \left(\frac{r_i - r}{\Delta r} \right), \qquad (1)$$

with Δr the bin size and $\sqcap(x)$ the unit pulse, which is equal to 1 for $-1/2 < x < 1/2$ and 0 elsewhere. This means that a fraction of $n(r)\Delta r$ of the ensemble is located at a distance to the nearest cloud edge between $r - 1/2\Delta r$ and $r + 1/2\Delta r$. $n(r)$ can be interpreted as the fractional area density and contains the cloud size distribution (for $r < 0$) and the void distance (the free path between two clouds) for $r > 0$. To avoid undersampling, we have chosen the bin size $\Delta r = 12\,\mathrm{m}$, slightly larger than the average sampling resolution of $10.6\,\mathrm{m}$. The mass flux density is

$$m(r) = \overline{w}(r)n(r), \qquad (2)$$

with $\overline{w}$ the conditionally averaged vertical velocity at r and with the mass density ρ omitted for brevity. By definition, integrating $n(r)$ from $-\infty$ to $+\infty$ yields 1. For a random flight pattern, $m(r)$ integrates to the expected value of 0. After a careful analysis of all flight data, we averaged all tracks within a layer of $300\,\mathrm{m}$. These windows are referred to with the mean height; so, for instance, the results of $650\,\mathrm{m}$ above the Earth's surface have been measured between $500\,\mathrm{m}$ and $800\,\mathrm{m}$.

The work of JHS08 used simulations based on the Small Cumulus Microphysics Study (SCMS). In comparison with the RICO observations we use, the differences in boundary conditions between the SCMS case and the RICO case is a possible source of differences. To eliminate this possibility, we compare the airplane observations with the LES intercomparison based on the RICO case as described by van Zanten et al. (2008). The numerical runs are performed using version 3 of the Dutch Atmospheric LES Heus et al. (DALES3; 2008b). We use $1024 \times 1024 \times 100$ gridpoints on a $12.8\,\mathrm{km} \times 12.8\,\mathrm{km} \times 4\,\mathrm{km}$ domain, resulting in a $12.5\,\mathrm{m} \times 12.5\,\mathrm{m} \times 40\,\mathrm{m}$ resolution. A time window of $24\,\mathrm{h}$ is simulated, of which the final $4\,\mathrm{h}$ is used for data collection. Distances to the cloud edge are obtained by calculating r in 2D as well as in the x-direction only, mimicking the 1D airplane observations. In the remainder of this paper, the word 'observations' always refers to the airplane observations, and never to the numerical results.

3. VALIDATION OF THE REFINED MASS-FLUX MODEL

The number density (Figure 1) and fractional mass flux $m\Delta r$(Figure 2) resulting from observations and from LES

are compared with each other. Since we are interested in a process driven by lateral mixing, we only present results for the middle region of the cloud layer, between $900\,\mathrm{m}$ and $1800\,\mathrm{m}$ above the surface. Outside this region, careful comparison is hampered by the precise location of cloud base and the inversion layer. The 2D results are very similar to the results of JHS08. As expected, there are some notable differences between the 2D and 1D results. By definition, the 1D probability density function $n(r)$ peaks at the cloud edge, since every in-cloud transect begins and ends at cloud edge, and the same can be said about every transect between two clouds. Such conditions need not to hold for the 2D number density, since in that case the number density is proportional to the distance to the nearest cloud center, and is bounded by the void distance between clouds. This results a maximum in Figure 1(a) around $500\,\mathrm{m}$ outside the cloud. The relatively short tail of the 2D pdf may be explained by the fact that clouds which are located alongside a flight track result in a small value for r in the 2D pdf, but are not taken into account in the 1D pdf's.

The main objective of this study can immediately be achieved with a qualitative look at Figure 2(c). Our results extracted from the airplane observations show a significant negative fractional mass flux at the cloud edge. Further away from the cloud the net mass flux is close to zero, despite the sizeable area of the far environment. Indeed, the number density in observations peaks much sharper at the cloud edge than even predicted by LES and consequently shows a larger near-cloud downward mass flux.

The relatively large number of points at the cloud edge in observations can be explained in at least two ways. First, the simulations mimic a truly random flight trajectory, whereas real flight campaigns generally aim at transecting more clouds. This is also illustrated by the wider tail on the cloud side and the smaller tail on the environmental side of Figure 1(c). These tail shapes mean that the observed cloud sizes were larger than in simulations, and void distances were smaller. In other words, the airplane aimed not only at transecting more clouds than would be the case for a random track, but also at penetrating those clouds near the center.

Another possible explanation for the large number of observed cloud edge points is that fluctuations in both velocity and liquid water content on scales below the LES grid size are consequently not taken into account in the simulations, but may give a sizeable contribution in observations. Even though the bin size is similar in observations and simulations, LES only samples averages over the entire gridbox, whereas the spread in possible values is much larger in observations.

By and large however, LES seems to give a good quantitative representation of the in-cloud mass flux, but discrepancies between simulations and observations in the number of near cloud-edge points are observed.

The accumulated mass flux for the entire cloud field

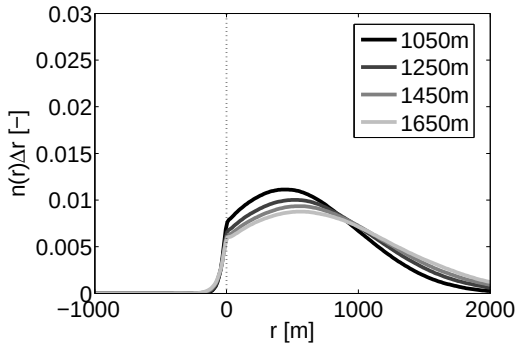

(a) 2D distances in simulations

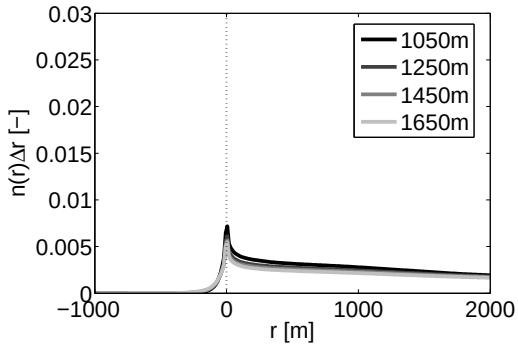

(b) 1D distances in simulations

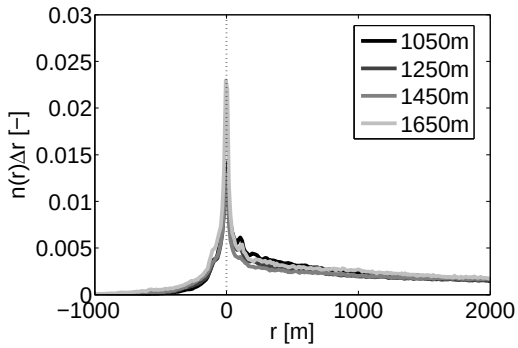

(c) 1D distances in airplane observations

FIG. 1: Number density function as a function of r for different observation levels.

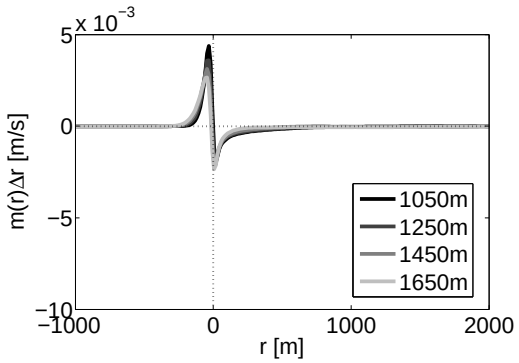

(a) 2D distances in simulations

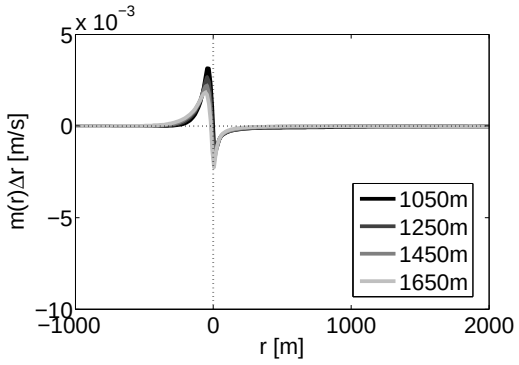

(b) 1D distances in simulations

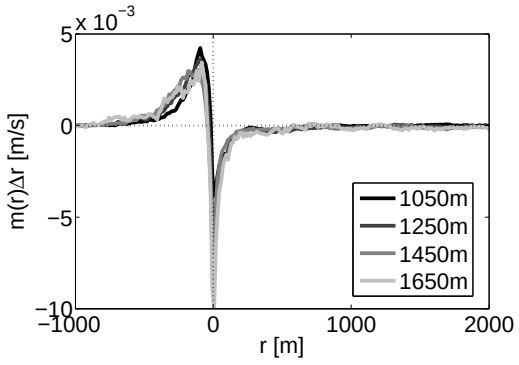

(c) 1D distances in airplane observations

FIG. 2: Fractional mass flux as a function of r for different observation levels.

$M(r)$

$$M(r) = \int_{-\infty}^{r} m(r')dr' \tag{3}$$

is presented in Figure 3. The total in-cloud mass flux M_c is equal to $M(r=0)$, since r is negative inside the cloud. By definition, $M(r)$ should go to zero for large r, but this can be a slow process for 1D distance calculation, and the sensitivity to a bias in the mass flux density is quite large. This is reflected by the mass flux for large r in observations for different heights, which ranges from stable or even somewhat increasing to sharply negative. Obviously, this should be interpreted rather cautiously. Qualitatively, observations and simulations result in a similarly shaped curve of M. However, the difference in the reported total in-cloud mass flux M_c is surprising. In figure Figure 3, this total in-cloud mass flux is denoted by the maximum value of M at the cloud edge $r=0$. According to LES, M_c is less than half of the value found in the observations. Of course, a difference in the in-cloud mass flux was to be expected from the difference in the fractional mass flux of figure Figure 2, and it is tempting to attribute it once again to the non-random flight track and to the contribution of very small clouds, but the discrepancy in such a key parameter remains somewhat surprising.

Summarizing, we see that it is non-trivial to obtain ironclad proof from the observational results alone that most of the in-cloud mass flux is compensated within a few hundred meters of the cloud edge. However, the observed fractional mass flux behaves as expected and clearly shows the role of the subsiding shell as predicted by JHS08. Furthermore, the agreement between the results obtained from observations and the 1-dimensional interpretation of LES give confidence that the 2-dimensional interpretation of the LES results of JHS08 is correct.

4. A CLOSER LOOK AT THE UP- AND DOWNDRAFTS

So far, we concentrated primarily on downdrafts near the edge of the cloud. In this section, also the occurrence of up- and downdrafts deeper inside the cloud as well as in the far environment are treated. In Figure 6, only the total fractional mass flux is presented. While these results show that on average the far environment has a negligible velocity, this does not mean that the air in this region remains motionless. Likewise, the net positive fractional mass flux inside the cloud is the sum of up- and downdrafts. To better study these up- and downdrafts, we need to further condition the sampling to updrafts ($w_i > 0$, denoted with a $+$) and downdrafts ($w_i < 0$, denoted with a $-$). Thus we define an up- and downdraft number fraction

$$n^{\pm}(r)\Delta r = \frac{1}{N(z)} \sum_{i}^{N(z)} \sqcap \left(\frac{r_i - r}{\Delta r} \right) H(\pm w_i), \tag{4}$$

a conditional average velocity

$$\overline{w}^{\pm}(r) = \frac{1}{n^{\pm}} \sum_{i}^{N(z)} w_i \sqcap \left(\frac{r_i - r}{\Delta r} \right) H(\pm w_i), \tag{5}$$

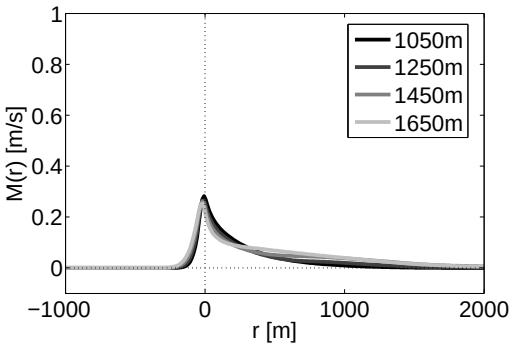

(a) 2D distances in simulations

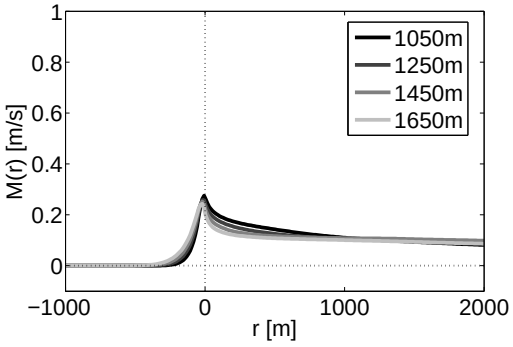

(b) 1D distances in simulations

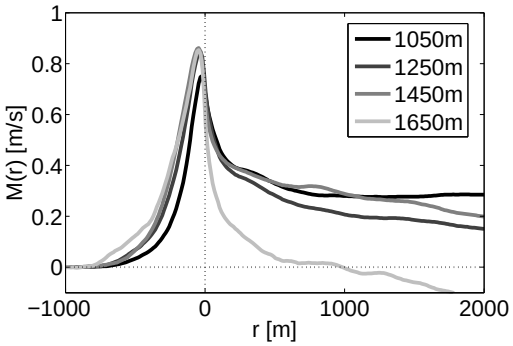

(c) 1D distances in airplane observations

FIG. 3: Accumulated mass flux as a function of r for different observation levels.

and a conditional mass flux density:

$$m^{\pm}(r) = n^{\pm}(r)w^{\pm}(r), \tag{6}$$

with $\mathrm{H}(x)$ the Heaviside step function. By definition, $n^{+}(r) + n^{-}(r) = n(r)$. In Figure 4 the number fractions are presented for the $1450\,\mathrm{m}$ window, normalized with $n(r)$; thus, the two curves in Figure 4 add up to 1. The corresponding average upward and downward velocities are shown in Figure 5. In general the vertical velocity corresponds well between observations and simulations. The most notable difference is a larger separation between the observed average upward and downward velocities. This can be explained by the tendency of the finite LES-grid to average out sub-filter scale fluctuations of the velocity field. In-cloud downward motions are only a little smaller than the motions at the cloud edge. Judging from the similarity between Figure 5(b) and Figure 5(c), these downdrafts seem to be quite well captured by LES. Many of the downdrafts may be located close to the cloud edge; as can be seen in Figure 4(a), the number of downdrafts goes rapidly to zero in 2D. Apart from these resolved downdrafts, the neglected sub-filter scale turbulent fluctuations in LES result in a narrower w distribution. This narrow distribution results in a decreased number of downdrafts inside the cloud. Indeed, this explains that inside the cloud the relative fraction of downdrafts as reported by LES in Figure 4(b) is smaller than 10% while the relative fraction of downdrafts in observations hovers around 20% (Figure 4(c)).

Another difference between observations and simulations is a sharper transition between cloud (or more precisely, the cloud core), shell and far environment in the simulations than in the observations, that can be seen in both the average velocity and especially in the fractional number density. These sharp transitions in simulations can be explained by the more homogeneous appearance of clouds in LES than in reality, not only because of the filtering of velocity fluctuations in LES, but since the moisture field is also filtered, small clouds or short dry transects within a cloud are also neglected in LES.

The results of Figure 4 and Figure 5 culminate in the conditional fractional mass flux as depicted in Figure 6. By and large, the fractional mass flux follows the trend of the vertical velocity; within the cloud, the total mass flux is close to the updraft flux, around the edge the downdrafts are dominated, and in the far environment the upward and downward mass flux cancel out each other. This tendency of the total mass flux to follow the dominant conditional mass flux is exaggerated by LES. The more diffuse transitions between cloud, shell and far environment in the observational results are again reflected in Figure 6.

The coherency of the flow is investigated with the help of the normalized structure function

$$D(r,z) = \frac{\overline{(w(z) - w(z_0))^2}}{\sigma_w^2(r, z_0)}, \tag{7}$$

with $z_0 = 1450\,\mathrm{m}$ the reference height and σ_w^2 the variance of the vertical velocity. The structure function can be

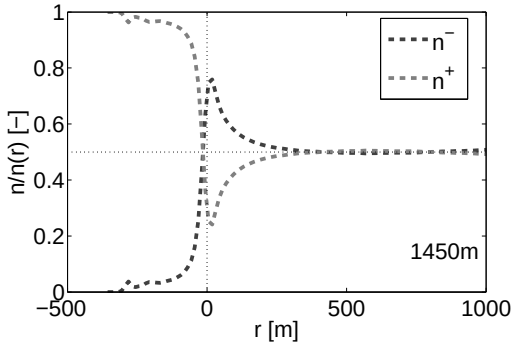

(a) 2D distances in simulations

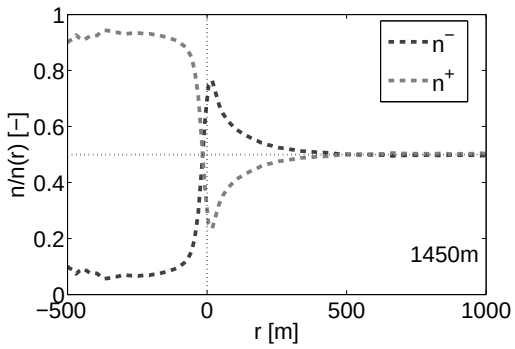

(b) 1D distances in simulations

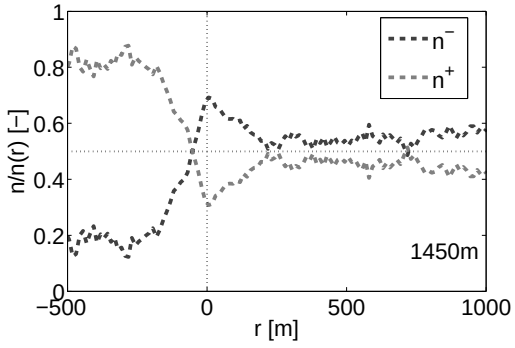

(c) 1D distances in airplane observations

FIG. 4: Up- and downward number fraction at $1450\,\mathrm{m}$. The light dashed line is the fraction of updrafts, the dark dashed line is the fraction of downdrafts.

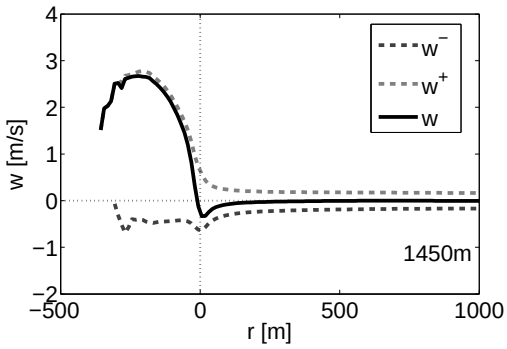

(a) 2D distances in simulations

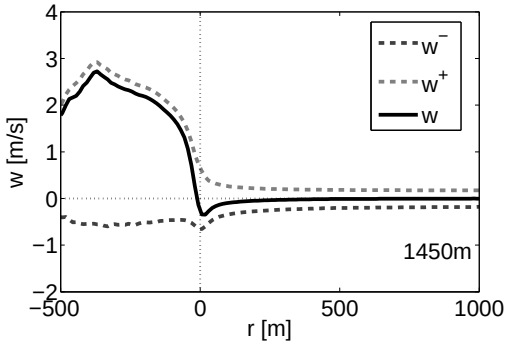

(b) 1D distances in simulations

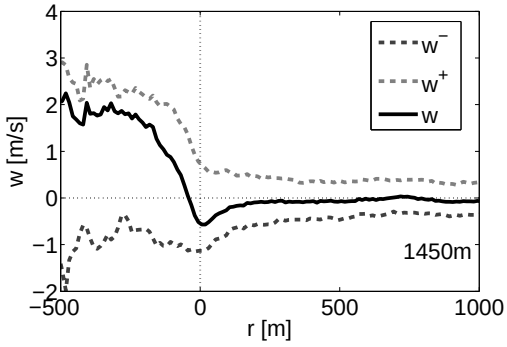

(c) 1D distances in airplane observations

FIG. 5: Conditional averaged vertical velocity as a function of r at $1450\,\mathrm{m}$. The light dashed line is the average velocity of the updrafts, the dark dashed line is the average velocity of the downdrafts. The full line denotes the unconditionally averaged vertical velocity.

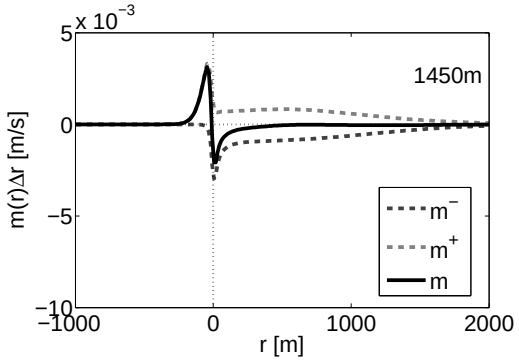

(a) 2D distances in simulations

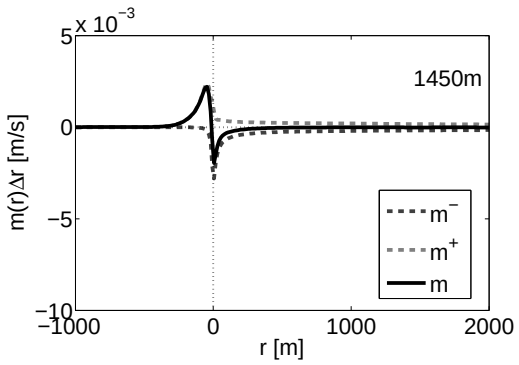

(b) 1D distances in simulations

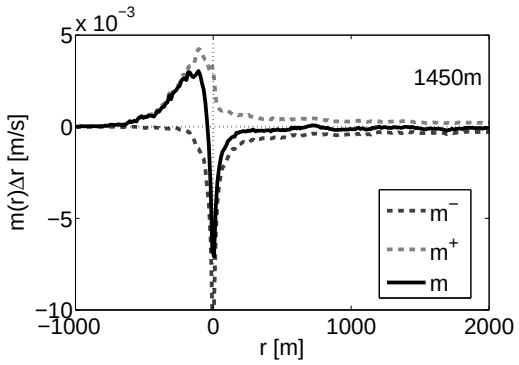

(c) 1D distances in airplane observations

FIG. 6: The conditional fractional mass flux as a function of r at $1450\,\mathrm{m}$. The light dashed line is the updraft mass flux, the dark dashed line is the mass flux of the downdrafts. The black line denotes the total fractional mass flux.

seen as the normalized difference in some field between two spatially separated points, and so gives a measure for the coherent length scales of the field. A structure function conditionally sampled over updrafts or downdrafts is defined as

$$D^{\pm}(r,z) = \frac{\overline{\left(w(z) - w^{\pm}(z_0)\right)^2}}{\sigma_w^2(r,z_0)}, \tag{8}$$

where, again, $+$ denotes the updrafts and $-$ denotes the downdrafts. Since the height dependent information could not be obtained from the airplane observations, the structure functions were obtained from LES (with r calculated in 2D). They are plotted in Figure 7. What immediately strikes the eye is the strong coherency in the in-cloud downdrafts. With the small-scale fluctuations removed from the conditional sampling, only the penetrating downdrafts remain. Although these downdrafts are scarce and do not contribute much to the mass flux, they clearly do exist and - if present - are able to maintain themselves over a considerable distance. There is also a clear asymmetry in the height visible in the in-cloud downdrafts in Figure 7(c). The most probable cause of this asymmetry lies in the location of the cloud top. By definition, the local cloud top is somewhere, at varying height, above z_0 for the points where $r < 0$. Cloud top clearly destroys the coherency of the flow. Since cloud base is located far below z_0 and is more or less constant for all clouds, such an effect does not happen for the coherency with the flow below z_0.

The in-cloud updrafts on the other hand appear to be much less coherent. This can be explained by the very turbulent nature of the cloud. Since the average in-cloud velocity is larger than zero, the turbulent fluctuations centered around the cloud-mean velocity are almost exclusively accounted for in the updraft structure function of Figure 7(b). The in-cloud downdrafts need to be quite intense to counteract the mean upflow in clouds, and because of that high intensity, the downdrafts are also more vertically coherent. So in contrast with the downdrafts, the turbulence emphasizes some smaller length scales in the in-cloud updrafts. Because of the predominance of the updrafts inside the cloud, the unconditionally sampled structure function is very similar to the structure function sampled over updrafts only.

In the far environment, the updrafts and downdrafts are similar to each other. Although on average not much is happening, the reduced turbulence and flow patterns like buoyancy waves allow for coherency over relatively large height differences.

Within the shell, around the edge of the cloud, a maximum in turbulence has been observed before (see Siebert et al., 2006; Heus and Jonker, 2008); this maximum is here expressed in the small coherent length scales at cloud edge. This is especially true for the updrafts, since in addition to the increased turbulence, there is not much mean coherent upflow appearant in the shell. For downdrafts, the coherency is somewhat larger, although, as was shown by Heus et al. (2008a), the Lagrangian dispersion in the shell only extends to about

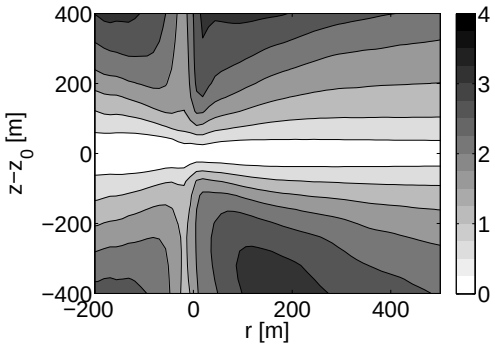

(a) $D(r, z)$

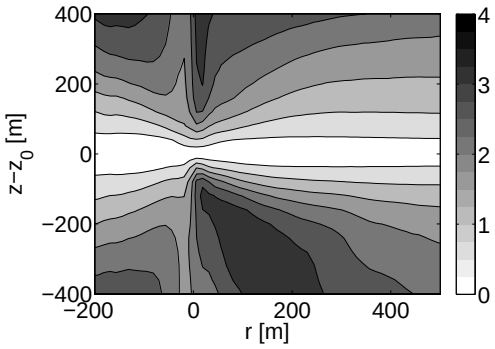

(b) $D^+(r, z)$

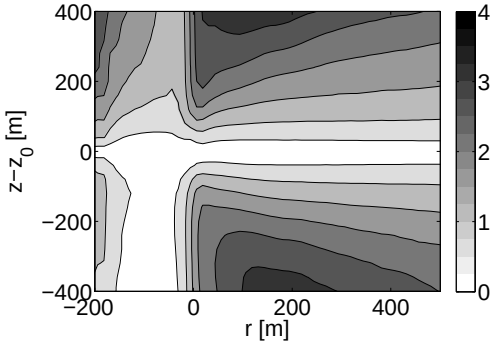

(c) $D^-(r, z)$

FIG. 7: The normalized structure function $D(r, z)$ as function of r and distance-to-reference-height $z_0 = 1450\,\mathrm{m}$. Obtained from LES.

Table 2: Transport properties of the cloud core, the shell and the far environment at $1450\,\mathrm{m}$.

	Area [%]	$\overline{w}$ [m s^{-1}]	M [10^{-3} m s^{-1}]
LES, 2D distances			
Cloud core	0.74	1.88	13.9
Shell	11	-0.060	-6.64
Env.	88	-0.0083	-7.29
LES, 1D distances			
Cloud core	0.85	1.76	14.9
Shell	8.7	-0.069	-5.96
Env.	90	-0.0092	-8.40
Observations, 1D distances			
Cloud core	6.2	1.10	68.5
Shell	9.4	-0.39	-36.6
Env.	84	-0.060	-50.4

$200\,\mathrm{m}$.

In Figure 8 we show the probability density function p of the vertical velocity conditionally sampled over the cloud core, the shell and the far environment, respectively. In accordance with the results from e.g., Figure 4(c), the shell is here defined as the region where $-50\,\mathrm{m} < r < 150\,\mathrm{m}$, and consequently the cloud core as $r < -50\,\mathrm{m}$ and the far environment as $r > 150\,\mathrm{m}$. We emphasize that the inner region is now not the entire cloud anymore, but only the part of the cloud with upward velocity, in other words, the cloud core. As noted before, the exact location of the borders does not entirely coincide with the location of the shell in LES. This is reflected in some minor variations between the plots, but the general picture obtained from the 3 panels in Figure 8 is very much similar and confirms the results presented above. The pdf of the far environment is a slender bell-shaped curve with a mean at $w = 0$. The shell and the cloud core show much larger variance, and also a strong skewness that is responsible for a deviation of the mean from the mode. Indeed, the strong but relatively rare up- and downdrafts are the entities that ultimately characterize the flow in the core and the shell. To fully appreciate the role of the cloud core, the shell and the far environment, the fractional areas of the 3 regions are reported in Table 2, along with the average velocity and the resulting fractional mass flux of each region. Clearly, while the area of the far environment is dominating over the area of the cloud and the area of the shell, the average velocity in the far environment is close to zero and a large part of the negative mass flux is concentrated in the shell.

5. CONCLUSIONS

In this study, the role of the subsiding shell around cumulus clouds was investigated by compositing airplane data with respect to the edge of the cloud, with focus on mass flux rather than on velocities. The role of the

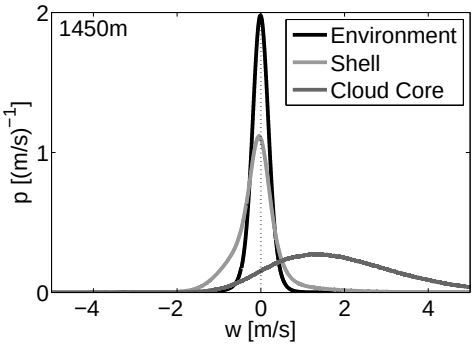

(a) 2D distances in simulations

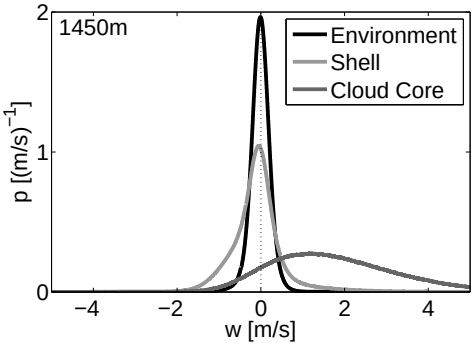

(b) 1D distances in simulations

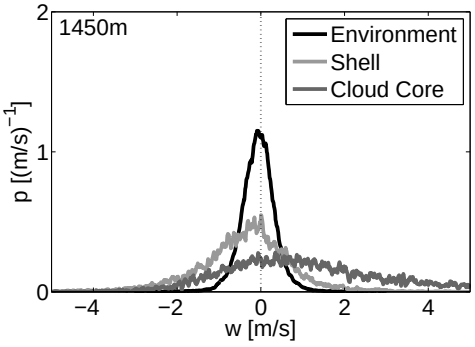

(c) 1D distances in airplane observations

FIG. 8: Probability density function of the vertical velocity in the far environment (black line), the shell (light gray) and the cloud core (dark gray).

shell in the balance between the upward in-cloud mass flux and the downward mass flux outside the cloud was clearly confirmed. As observed before in LES, the shell is responsible for a large part of the environmental downward mass flux. The one-dimensional character of the airplane observations somewhat complicates interpretation of the velocity measurements in the context of a cloud shell. However, the role of the shell appears, if anything, even stronger in observations than predicted by LES. As in LES, careful compositing of the observations relative to the cloud edge and sufficient sampling to average out the turbulence turn out to be key factors in revealing the role of the shell in transporting mass. The theoretical understanding of the mechanisms behind the shell alongside the various studies of single clouds surrounded by a shell leads to the conviction that the role of the subsiding shell in the mass-flux balance can be observed in many more data sets, provided that the appropriate analysis is carried out.

LES seems to be able to go well beyond qualitative insights and to quantitatively predict the velocity distribution and the mass flux density in and around a shallow cumulus cloud. Differences between simulations and observations can mostly be seen in the underprediction of downdrafts at the cloud edge, and in the smaller variation in vertical velocity due to the discrete grid of LES. The overall probability density function of the vertical velocity w is dominated by a single peak at $w = 0$. However, for a correct understanding and modeling of the physics of the cloud layer, it is essential to interpret the pdf as trimodal: A large portion (the far environment) with negligible vertical velocity, and two small areas (the core and the shell) that approximately balance each other out.

The overall behavior of updrafts and downdrafts in and around the cloud, including their coherency and their transport of species remains to conceil many fascinating mechanisms. Not all of them could be treated here, and some could only be speculated upon within the framework of this paper. In other words, the dynamics of cumulus clouds is still, and probably will remain for quite some time, an interesting alley of research.

Acknowledgments We would like to thank Bjorn Stevens (UCLA) for his suggestions to look into in-cloud downdrafts. The investigations were supported by the Netherlands Organization for Scientific Research (NWO). This work was sponsored by the National Computing Facilities Foundation (NCF) for the use of supercomputer facilities. The National Center for Atmospheric Research is sponsored by the National Science Foundation.

REFERENCES

Asai, T., and A. Kashara, 1967: A theoretical study of compensating downward motions associated with cumulus clouds. *J. Atmos. Sci.*, **24**(5), 487–496.

Blyth, A. M., W. A. Cooper, and J. B. Jensen, 1988: A study of the source of entrained air in Montana cumuli. *J. Atmos. Sci.*, **45**(24), 3944–3964.

Gerber, H., G. Frick, J. B. Jensen, and J. G. Hudson, 2008: Entrainment, mixing, and microphysics in trade-wind cumulus, submitted.

Grabowski, W. W., and T. L. Clark, 1991: Cloudenvironment interface instability: Rising thermal calculations in two spatial dimensions. *J. Atmos. Sci.*, **48**(4), 527–546.

Grabowski, W. W., and T. L. Clark, 1993a: Cloud-environment interface instability: Part II: Extension to three spatial dimensions. *J. Atmos. Sci.*, **50**(4), 555–573.

Grabowski, W. W., and T. L. Clark, 1993b: Cloud-environment interface instability. Part III: Direct influence of environmental shear. *J. Atmos. Sci.*, **50**(23), 3821–3828.

Heus, T., and H. J. J. Jonker, 2008: Subsiding shells around shallow cumulus clouds. *J. Atmos. Sci.*, **65**(3), 1003–1018.

Heus, T., G. van Dijk, H. J. J. Jonker, and H. E. A. van den Akker, 2008a: Mixing in shallow cumulus clouds studied by Lagrangian particle tracking. *J. Atmos. Sci.*. In press.

Heus, T., et al., 2008b: An overview of Dutch Atmospheric LES, in preparation.

Jonas, P. R., 1990: Observations of cumulus cloud entrainment. *Atmos. Res.*, **25**, 105–127.

Jonker, H. J. J., T. Heus, and P. P. Sullivan, 2008: A refined view on vertical transport by cumulus convection. *Geophys. Res. Lett.*, **35**, L07,810.

Lenschow, D. H., M. Zhou, X. Zeng, L. Chen, and X. Xu, 2000: Measurements of fine-scale structure at the top of marine stratocumulus. *Bound.-Layer Meteor.*, **97**(97), 331–357.

Paluch, I. R., 1979: The entrainment mechanism in Colorado cumuli. *J. Atmos. Sci.*, **36**, 2467.

Rauber, R. M., et al., 2007a: Rain in (shallow) cumulus over the ocean - The RICO campaign. *Bull. Amer. Meteor. Soc.*, **88**(12), 1912–1928.

Rauber, R. M., et al., 2007b: Supplement to: Rain in (shallow) cumulus over the ocean - The RICO campaign. *Bull. Amer. Meteor. Soc.*, **88**(12), S12–S18.

Rodts, S. M. A., P. G. Duynkerke, and H. J. J. Jonker, 2003: Size distributions and dynamical properties of shallow cumulus clouds from aircraft observations and satellite data. *J. Atmos. Sci.*, **60**(16), 1895–1912.

Siebert, H., K. Lehmann, M. Wendisch, and R. Shaw, 2006: Small-scale turbulence in clouds. *12th Conference on Cloud Physics, 10 - 14 July, Madison, WI, USA.*.

Squires, P., 1958: The microstructure and colloidal stability of warm clouds 1. The relation between structure and stability. *Tellus*, **10**(2), 256–261.

Stommel, H., 1947: Entrainment of air into a cumulus cloud. *J. Meteor.*, **4**, 91–94.

Taylor, G. R., and M. B. Baker, 1991: Entrainment and detrainment in cumulus clouds. *J. Atmos. Sci.*, **48**(1), 112–121.

van Zanten, M. C., et al., 2008: Rico intercomparison, in preparation.